Nuclear Physics B168 (1980) 477–494

LUMINOSITY FUNCTIONS FOR TWO-PHOTON PROCESSES IN e^+e^- COLLISIONS

J.H. FIELD

Deutsches Elektronen-Synchrotron DESY, Hamburg, Germany

Received 21 January 1980

An analysis is given of the QED factors relating the cross section for $ee \to eeX$ to the virtual 2-photon collision $\gamma^*\gamma^* \to X$. Only transverse photons are considered, but no kinematical approximations are made. The cases where none, one or both of the scattered electrons are detected at angles $\gg m_e/E$ (E = beam energy) are separately considered. A full discussion is given of the kinematical restrictions necessary to arrive at factorisible equivalent photon approximation formulae, and quantitative comparisons are given. Also discussed are the rapidity distribution of the produced system X and restrictions on the effective two-photon luminosity due to angular cuts on produced particles.

1. Introduction

The aim of this paper is to present an analysis, useful for experimental applications, of the purely QED factors relating an observed process of the type

$$ee \to eeX \tag{1}$$

(the symbol "e" and the term "electron" below stand for electrons of arbitrary charge) to the elementary photon-photon process

$$\gamma^*\gamma^* \to X\,, \tag{2}$$

where X is any produced system of invariant mass W, but otherwise unspecified. This problem has already been treated extensively in the literature [1–4]; not always however correctly*, often with a rather theoretical bias and with the emphasis mainly on total cross sections for process (1). The present work aims to be more experimentally orientated and to concentrate particularly on the connection between the processes (1) and (2) when the scattered electrons (one or both) are detected or "tagged" at angles θ such that:

$$m_e/E \ll \theta \ll 1$$

(E = beam energy, m_e = electron mass). However, the interesting question of the total cross section is also considered in some detail.

* There is a thorough discussion of various incorrect derivations of equivalent photon spectra for two-photon collisions in section 6.7 of ref. [5].

The analysis is given in terms of differential photon-photon luminosity functions $d\mathcal{L}/dz$*, where z is the scaled effective mass: $z \equiv W/2E$, of the system X. The starting point is the general analysis of the connection between processes (1) and (2) in terms of helicity amplitudes for the virtual photons [3, 4]. The implicit assumption made here is that the process (1) proceeds only via the Feynman graph shown in fig. 1. For example bremsstrahlung graphs, where the system X is produced by a single virtual photon are neglected. The connection between processes (1) and (2) is then given by the equation

$$\frac{d^6\sigma}{dv_1 \ldots dv_6} = \sum_{ij} \frac{d^6\mathcal{L}^{ij}}{dv_1 \ldots dv_6} \sigma_{ij}(W^2, q_1^2, q_2^2), \tag{3}$$

where $d^6\sigma/(dv_1 \ldots dv_6)$ is the cross section for process (1) and σ_{ij} that for process (2). $v_1 \ldots v_6$ are 6 variables kinematically defining the configuration of the scattered electrons; $-q_1^2, -q_2^2$ are the masses of the two virtual photons with polarization indices i and j. Three further assumptions are made to arrive at a definition of a single luminosity function $d\mathcal{L}/dz$:

(i) only transverse virtual photons are considered:

$$ij = TT, \qquad d\mathcal{L}/dz \equiv d\mathcal{L}^{TT}/dz \ ;$$

(ii) the photon mass dependence of σ_{TT} is neglected:

$$\sigma_{TT}(W^2, q_1^2, q_2^2) = \sigma_{TT}(W^2, 0, 0) \equiv \sigma(W^2) .$$

(iii) as the azimuthal angles of the scattered electrons are, in all cases, integrated over, terms proportional to the relative polarization of the transverse photons are neglected.

These three assumptions are also essential in derivations of the "Weizsäcker–Williams" or "equivalent photon approximation" (EPA) photon energy spectra [7–13], but the analysis given here is more general. The luminosity function considered here does not in general split into a product of two photon flux factors

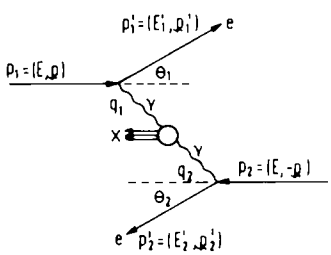

Fig. 1. Definitions of kinematic quantities.

* Note that the definition of the two-photon luminosity function used here is somewhat different to that given in ref. [6]. The rate for process (1) is given by:

ee luminosity × the luminosity function × cross section for (2).

each containing the kinematical variables of only one of the scattered electrons. The relationship of the present analysis to EPA calculations is discussed in sect. 6.

With (i) to (iii), eq. (3) simplifies to

$$\frac{\mathrm{d}^6\sigma}{\mathrm{d}v_1 \ldots \mathrm{d}v_6} = \frac{\mathrm{d}^6\mathscr{L}}{\mathrm{d}v_1 \ldots \mathrm{d}v_6}\,\sigma(W^2)\,. \tag{3a}$$

$\mathrm{d}\mathscr{L}/\mathrm{d}z$ is then found from the full differential expression, eq. (3a), by integrating over the scattered electron variables, applying suitable cuts when luminosity functions for double tagging (DT) or single tagging (ST) are required. Assumption (ii) is essential to carry out this integration and the resulting function $\mathrm{d}\mathscr{L}/\mathrm{d}z$ is only physically meaningful [unlike the fully differential function in eq. (3a)] if (ii) is true. To go beyond this requires detailed knowledge of the physics of process (2). If the photon coupling is pointlike, assumption (ii) is likely to be a good approximation. For VDM type couplings to hadronic systems and for large beam energies, large suppressions of the cross section (2) are expected. This point is further discussed in sect. 7 below. Throughout this paper the virtual photon-photon cross section is assumed to be independent of q_1^2, q_2^2.

The organization of the following sections of the paper is as follows: in the sect. 2 definitions of kinematical variables are given. Sects. 3, 4 and 5 treat successively the cases of untagged, double tagged and single tagged luminosity. Sect. 6 discusses factorizable (EPA) formulae for the luminosity functions. In sect. 7 the rapidity distribution of the luminosity is briefly considered, and in sect. 8 modifications of the effective luminosity due to acceptance requirements on the produced system X are calculated. Sect. 9 contains a summary of the essential conclusions and a few remarks relating this study to other recent work.

2. Definitions and kinematics

The 4-vectors of the incoming and scattered electrons in the lab system are defined in fig. 1. θ_1 and θ_2 are the electron lab scattering angles and ϕ is the azimuthal angle between the planes defined by the beam direction and the two scattered electrons.

Other definitions are:

$$\left.\begin{aligned} x_i &\equiv (E - E_i')/E = \text{scaled photon energy} \\ Q_i^2 &\equiv q_i^2/4E^2 = -(\text{scaled photon mass})^2 \end{aligned}\right\} i = 1, 2\,,$$

$$W^2 \equiv -(q_1 + q_2)^2 = (\gamma\gamma \text{ effective mass})^2\,,$$

$$z \equiv W/2E\,, \qquad \sigma \equiv z^2\,,$$

$$m_e \equiv \text{electron mass}\,,$$

$$\cos\Theta \equiv \boldsymbol{p}_1 \cdot \boldsymbol{p}_2/|\boldsymbol{p}_1||\boldsymbol{p}_2| = \sin\theta_1 \sin\theta_2 \cos\phi - \cos\theta_1 \cos\theta_2\,.$$

The $\gamma\gamma$ effective mass is given, in terms of the scattered electron variables, by the expression (neglecting m_e^2 compared to $p_1'^2$, $p_2'^2$)

$$z^2 = x_1 x_2 - \tfrac{1}{2}(1-x_1)(1-x_2)(1+\cos\Theta)\,. \tag{4}$$

3. Untagged luminosity

In this case $\mathrm{d}\mathscr{L}/\mathrm{d}z$ is given by integrating $\mathrm{d}^6\mathscr{L}/(\mathrm{d}v_1 \ldots \mathrm{d}v_6)$ over the complete phase space of the scattered electrons. The result has already been given in ref. [4]. It may be written as

$$\frac{\mathrm{d}\mathscr{L}^{\mathrm{TOT}}}{\mathrm{d}z} = 2\left(\frac{\alpha}{\pi}\right)^2 \frac{1}{z}\left[F^{(1)}(E/m_e, \sigma) + F^{(2)}(\sigma) + F^{(3)}(\sigma)\right], \tag{5}$$

where the functional dependences of the three terms are as indicated. The full expressions for $F^{(1)}$, $F^{(2)}$ are rather complicated and are given in the appendix. All the logarithmic terms are contained in $F^{(1)}$ and $F^{(2)}$. $F^{(3)}$, which contains only powers of σ and constants, is negligible – it vanishes for $\sigma = 1$ and gives only a fraction of a percent correction near $\sigma = 0$. Curves of $\mathrm{d}\mathscr{L}^{\mathrm{TOT}}/\mathrm{d}z$ for $E = 15$, 100, 1000 GeV are shown in fig. 2. Only the $F^{(1)}$, $F^{(2)}$ terms are included. The contributions from the powers of $\ln(1/\sigma)$, $\ln(1-\sigma)$ are important. Retaining only the $(\ln(2E/m_e))^2$, $\ln(2E/m_e)$ terms leads to a negative luminosity for $z > 0.85$! However,

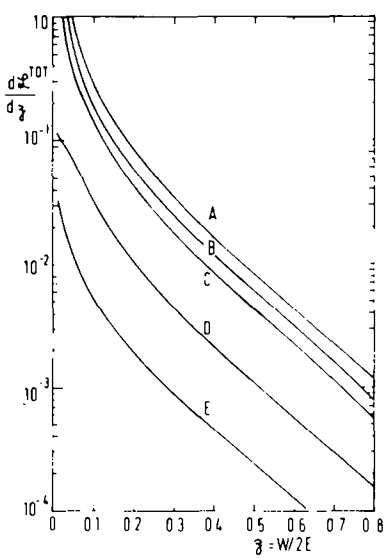

Fig. 2. Two-photon differential luminosity curves. Curves A, B, C: Total luminosity for $E = 1000$, 100, 15 GeV. Curve D: Single tagged luminosity for tagging in $0 < \phi < 2\pi$, $20 < \theta < 200$ mrad, $E = 15$ GeV. Curve E: Double tagged luminosity for tagging in $0 < \phi < 2\pi$, $20 < \theta < 200$ mrad, $E = 15$ GeV.

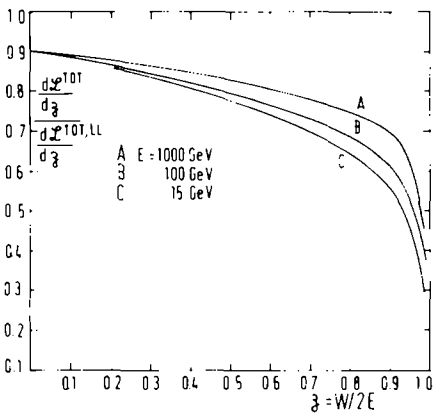

Fig. 3. Ratio of total differential luminosity to the leading log approximation, eq. (6). Curves A, B, C for $E = 1000, 100, 15$ GeV.

taking only the leading logarithmic term in $\ln(2E/m_e)$ in $F^{(1)}$ in eq. (5), i.e.,

$$\frac{\mathrm{d}\mathscr{L}^{\mathrm{TOT,LL}}}{\mathrm{d}z} = 4\left(\frac{\alpha}{\pi}\right)^2 \frac{1}{z}\left(\ln\frac{2E}{m_e}\right)^2\left\{2(1+\tfrac{1}{2}\sigma)^2 \ln\frac{1}{\sigma} - (1-\sigma)(3+\sigma)\right\}, \tag{6}$$

gives a reasonably good approximation (scale error $\simeq 10\%$ and about 10% variation) to the complete expression (5), except in the region of $\sigma = 1$. This is shown in fig. 3 where the ratio of $\mathrm{d}\mathscr{L}^{\mathrm{TOT}}/\mathrm{d}z$ relative to $\mathrm{d}\mathscr{L}^{\mathrm{TOT,LL}}/\mathrm{d}z$ is shown for $E = 15$, 100, 1000 GeV.

The function of σ in the curly brackets in eq. (6), first given by Low in 1960 [14], follows also from the Weizsäcker–Williams approximation, where it is assumed that the function $\mathrm{d}\mathscr{L}/\mathrm{d}z$ can be derived from the product of two photon flux factors one from each electron-γ vertex, the number $\mathrm{d}N_\gamma$ of virtual photons in the range $\mathrm{d}x$ of scaled photon energy being given by

$$\frac{\mathrm{d}N_\gamma}{\mathrm{d}x} = \left(\frac{\alpha}{\pi}\right)\frac{[1+(1-x)^2]}{x}\ln\frac{2E}{m_e}. \tag{7}$$

The functional form given in (6) follows on integrating the product of two flux factors of the form (7) over x_1, and x_2 subject to the constraint, which follows from (5) in the limit $\Theta \simeq \pi$

$$z^2 = \sigma \simeq x_1 x_2 . \tag{8}$$

4. Double tagged luminosity

The full expression for the completely differential luminosity function, eq. (9), follows on rewriting eqs. (28) and (29d) of ref. [4] in terms of the variables defined in

sect. 2 and using the definition of the luminosity function eq. (3):

$$\frac{d^5\mathcal{L}}{d\theta_1\, d\theta_2\, d\phi\, dx_1\, dx_2} = \frac{\alpha^2}{32\pi^3}\xi \cot\tfrac{1}{2}\theta_1 \cot\tfrac{1}{2}\theta_2 \times\left\{\frac{[K-2(x_2+Q_2^2)]^2}{\xi^2}+1-\frac{m_e^2}{E^2Q_1^2}\right\} \times\left\{\frac{[K-2(x_1+Q_1^2)]^2}{\xi^2}+1-\frac{m_e^2}{E^2Q_2^2}\right\}, \qquad (9)$$

where

$$K \equiv z^2+Q_1^2-Q_2^2,$$
$$\xi^2 \equiv K^2-4Q_1^2Q_2^2,$$

and, in limit $m_e^2/E^2 \ll Q_1^2, Q_2^2$

$$Q_i^2 = (1-x_i)\sin^2\tfrac{1}{2}\theta_i, \qquad i=1,2.$$

Eq. (9) contains 5 variables instead of 6 as in eq. (3a), as the trivial overall azimuthal rotation of the configuration about the beam axis has been integrated out.

For the calculation of luminosity for a practical range of tagging angles, $\theta_1, \theta_2 \gtrsim 10$ mrad, which is typical of experiments on the present PETRA/PEP generation of e^+e^- storage rings, one has, for double tagging (detection of both scattered electrons)

$$Q_1^2, Q_2^2 \gg m_e^2/E^2,$$

so the last terms in the two curly brackets of eq. (9) may be dropped. With this approximation the luminosity within a given angular range is independent of the beam energy. The double tagged luminosity with both scattered electrons detected in the angular range,

$$\theta_{\min} \leq \theta_1, \theta_2 \leq \theta_{\max}$$

($\theta_{\min} \gg m_e/E$), has been calculated by numerical integration of eq. (9)*. The integration is carried out over the 4 variables θ_1, θ_2, ϕ, x_1. x_2 is expressed in terms of z and these variables by using eq. (4). The integration contour on the x_1, x_2 plane for fixed z and different values of the angle Θ is shown in fig. 4. For $\Theta = \pi$ the contour is a hyperbola, for $\Theta = 0$ it is a line $z^2 = 1 - x_1 - x_2$. Results of this calculation are shown in fig. 2 (curve E) for $\theta_{\min} = 20$, $\theta_{\max} = 200$ mrad. In fig. 5, to better display the variation for the different angular ranges, the curves are normalised to the fully angular integrated luminosity in leading log approximation given by eq. (6). The curves are calculated for $E = 15$ GeV. As mentioned above the shape of the curves is

* The DESY Library numerical integration program QUINT (authors R. Noehre, O. Hell) was used.

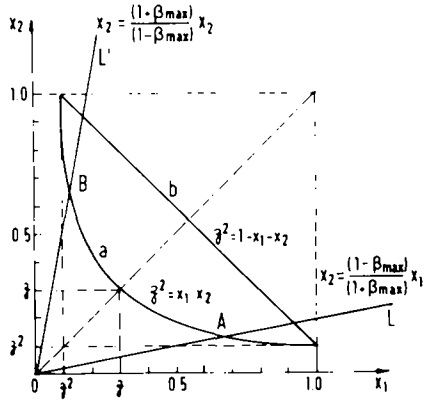

Fig. 4. Integration contours in the plane of scaled virtual photon energies x_1, x_2 for fixed scaled photon-photon invariant mass, z. Curve a: $z = 0.3$, $\Theta = \pi$. Curve b: $z = 0.3$, $\Theta = 0$. AB: Allowed integration range for $\beta < \beta_{max} = 0.682$.

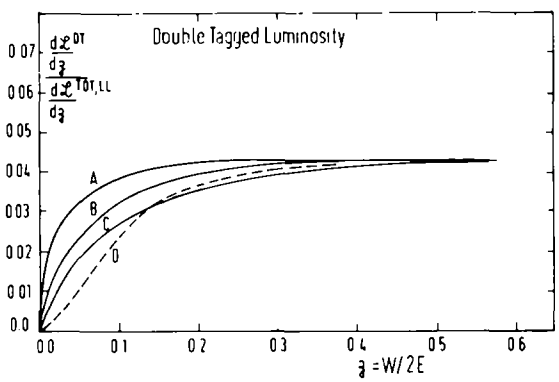

Fig. 5. Double tagging efficiency curves from integration of eq. (9). $E = 15$ GeV A: $10 < \theta_1, \theta_2 < 100$ mrad; B: $20 < \theta_1, \theta_2 < 200$ mrad; C: $30 < \theta_1, \theta_2 < 300$ mrad; D: $20 < \theta_1, \theta_2 < 200$ mrad. Integration contour: $z^2 = x_1 x_2$.

energy independent. The overall scale, from eq. (6) is given by $120(\ln(2E/m_e))^{-2}$ (E in GeV). The main qualitative features of the curves are:

(i) a suppression of the fractional luminosity accepted, which is in experimental terms, equivalent to double tagging efficiency:

$$\varepsilon_{DT} \equiv \frac{d\mathscr{L}^{DT}}{dz} \Big/ \frac{d\mathscr{L}^{TOT,LL}}{dz},$$

at small values of z;

(ii) ε_{DT} independent of z for $z \geq 0.5$;

(iii) the suppression becomes more severe at larger tagging angles.

The importance of using the full expression relating z^2 to x_1, x_2, eq. (4), instead of the approximate expression, eq. (8), is shown in fig. 5. The dotted curve D shows the luminosity function for $\theta_{\min} = 20$, $\theta_{\max} = 200$ mrad using eq. (8) instead of (4).

5. Single tagged luminosity

In principle the single tagged luminosity function could be found by numerical integration of eq. (9) over the full range of one of the scattered electrons, say $0 < \theta_1 < \pi$, restricting the angular range of the second electron as before to $\theta_{\min} < \theta_2 < \theta_{\max}$. Since, however, the dominant contribution to the θ_1 integration comes from very small angles $\theta_1 \simeq m_e/E$ it is simpler to do this integration analytically. The following approximations are then made to eq. (9):

(i) $Q_1^2 = 0$ in K, ξ and in the second curly bracket of eq. (9);

(ii) $Q_2^2 \gg (m_e/E)^2$ so the $m_e^2/E^2 Q_2^2$ term is dropped.

The θ_1 integral with x_1 fixed can then be written as an integral over Q_1^2 between the limits

$$Q_{\min}^2 = \frac{m_e^2}{4E^2}\left(\frac{x_1}{1-x_1}\right)^2 + O(m_e^4),$$

$$Q_{\max}^2 = 1 - x_1 .$$

The further approximation $\theta_1 \simeq 0$ is made in the relation, eq. (4), which then becomes

$$z^2 \simeq x_1 x_2 - \tfrac{1}{2}(1-x_1)(1-x_2)(1-\cos\theta_2) . \tag{10}$$

As the ϕ dependence of the integrand then vanishes, the ϕ integration is trivial, giving simply a factor 2π. On carrying out the Q_1^2 integration the following 3-fold differential luminosity function is found:

$$\frac{d^3\mathcal{L}}{d\theta_2\, dx_1\, dx_2} = \frac{\alpha^2}{8\pi^2} K' \cot\tfrac{1}{2}\theta_2 \left[\frac{(K'-2x_1)^2}{K'^2} + 1\right]$$
$$\times \left\{\left[\ln\frac{2E}{m_e}\frac{(1-x_1)}{x_1}\right]\left[\frac{\{K'-2(x_2+Q_2^2)\}^2}{K'^2} + 1\right] - 2\frac{(1-x_1)}{x_1^2}\right\}, \tag{11}$$

where $K' \equiv z^2 + Q_2^2$ and terms of order m_e^2/E^2 relative to unity have been dropped. $d\mathcal{L}^{ST}/dz$ is then given by an integral over x_1 and θ_2, using eq. (10) to eliminate x_2. The single tagged luminosity found in this way from eq. (11) is given for $\theta_{\min} = 20$, $\theta_{\max} = 200$ mrad, $E = 15$ GeV, by curve D of fig. 2. Fig. 6 shows curves for other angular ranges, normalized to $d\mathcal{L}^{TOT.LI.}/dz$ as in fig. 3. The same qualitative features (i)–(iii) mentioned above for the double tagged case are again evident here. In addition there is a slow fall-off as $z \to 1$. From fig. 3 it can be seen that this fall-off will be largely eliminated, at least up to $z \simeq 0.9$ if the full angle integrated luminosity is used for normalization instead of the leading log approximation to it. Also shown in

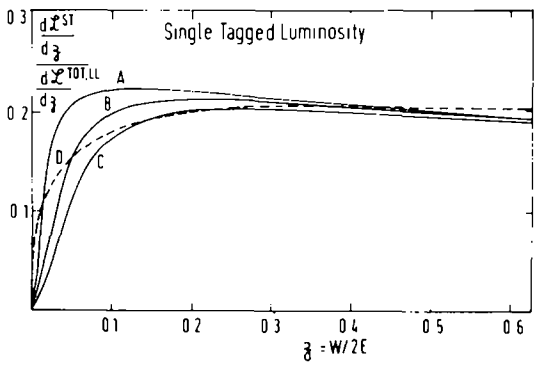

Fig. 6. Single tagging efficiency curves from integration of eq. (11). $E = 15$ GeV. A: $10 < \theta_2 < 100$ mrad; B: $20 < \theta_2 < 200$ mrad; C: $30 < \theta_2 < 300$ mrad; D: $20 < \theta_2 < 200$ mrad $\sqrt{\text{curve B in fig. 5.}}$

fig. 6 (dotted curve D) is $\sqrt{\varepsilon_{\mathrm{DT}}}$ for $\theta_{\min} = 20$, $\theta_{\max} = 200$ mrad, given by assuming "factorization" of the tagging efficiency. Except for values of $z \leqslant 0.05$ the agreement with curve B is quite good (10% level). It should be noted that the single tagging efficiency defined by the curves in fig. 6 corresponds to tagging in one direction only. Use of both forward and backward detectors will give double the efficiency. It can be seen from eq. (11) that the single tagged luminosity will scale with energy $\propto \ln(2E/m_e)$ at high energies, where the logarithmic term in the large curly bracket of eq. (11) dominates. The tagging efficiency, defined as

$$\varepsilon_{\mathrm{ST}} \equiv \frac{\mathrm{d}\mathscr{L}^{\mathrm{ST}}}{\mathrm{d}z} \Big/ \frac{\mathrm{d}\mathscr{L}^{\mathrm{TOT,LL}}}{\mathrm{d}z}$$

will then scale $(\ln(2E/m_e))^{-1}$.

6. Factorizable formulae: Weizsäcker-Williams approximation

The condition to derive factorizable formulae from the general expression eq. (9) is that

$$z^2 \gg Q_1^2, Q_2^2 . \tag{12}$$

From the definitions of Q_1^2 and Q_2^2 this implies that $\theta_{1,2} \ll 1$ or $x_{1,2} \simeq 1$ and hence, from eq. (4), that eq. (8) is closely satisfied. Making this approximation the following expressions are found for the luminosity functions differential in x_1 and x_2:

$$\frac{\mathrm{d}^2\mathscr{L}^{\mathrm{TOT}}}{\mathrm{d}x_1\,\mathrm{d}x_2} = \frac{\mathrm{d}N_\gamma^{\mathrm{TOT}}}{\mathrm{d}x_1}(x_1) \cdot \frac{\mathrm{d}N_\gamma^{\mathrm{TOT}}}{\mathrm{d}x_2}(x_2) , \tag{13a}$$

$$\frac{\mathrm{d}^2\mathscr{L}^{\mathrm{ST}}}{\mathrm{d}x_1\,\mathrm{d}x_2} = \frac{\mathrm{d}N_\gamma^{\mathrm{TOT}}}{\mathrm{d}x_1}(x_1) \cdot \frac{\mathrm{d}N_\gamma}{\mathrm{d}x_2}(x_2, \theta_{\min}, \theta_{\max}) , \tag{13b}$$

$$\frac{d^2\mathscr{L}^{DT}}{dx_1\,dx_2} = \frac{dN_\gamma}{dx_1}(x_1, \theta_{min}, \theta_{max}) \cdot \frac{dN_\gamma}{dx_2}(x_2, \theta_{min}, \theta_{max}) . \tag{13c}$$

where

$$\frac{dN_\gamma^{TOT}}{dx} = \left(\frac{\alpha}{\pi}\right)\frac{1}{x}\left\{\left[\ln\frac{2E}{m_e}\frac{(1-x)}{x}\right][1+(1-x)^2]-1+x\right\}, \tag{14}$$

$$\frac{dN_\gamma}{dx}(x, \theta_{min}, \theta_{max}) = \left(\frac{\alpha}{\pi}\right)\frac{[1+(1-x)^2]}{x}\ln\frac{\theta_{max}}{\theta_{min}} . \tag{15}$$

Here it is assumed that $\sin\theta \simeq \theta$ and $\theta_{min}^2 \gg (m_e/E)^2$. Eqs. (13a), (13b), (13c) correspond to the total, single tagged and double tagged luminosities, respectively. Eq. (13a) is derived from eq. (9) by integrating over both Q_1^2 and Q_2^2, instead of over Q_1^2 only, as in the derivation of eq. (11); retaining is this case both of the $m_e^2/E^2Q_i^2$ terms. Eq. (13b) is derivable directly from eq. (11) on integrating over θ_2. Eq. (13c) is given by eq. (9) on dropping the $m_e^2/E^2Q_i^2$ terms and integrating over θ_1 and θ_2. In all cases condition (12) allows the replacement

$$K = K' = z^2 .$$

Making the leading logarithm approximation that:

$$\ln\frac{2E}{m_e} \gg \ln\frac{(1-x)}{x}, \qquad \ln\frac{2E}{m_e} \gg 1-x ,$$

the expression for dN_γ^{TOT}/dx reduces to that given in eq. (7). With this approximation $dN_\gamma^{TOT}(x)/dx$ and $dN_\gamma(x, \theta_{min}, \theta_{max})/dx$ have identical x dependence and carrying out the integration over one of the photon energies for fixed z leads to the Low function, eq. (6), for the variation of $d\mathscr{L}/dz$ with z.

In calculating dN_γ^{TOT}/dx, since the most important contributions come from small angles $\simeq m_e/E$ in the angular integration, the condition (12) is well satisfied and it is not suprising that the luminosity function calculated by convolution of independent photon flux factors, which is the philosophy adopted in the Weizsäcker–Williams, or equivalent photon approximation, gives a good approximation to the exact luminosity function eq. (9). In this limit also, the restriction to transverse photons is expected to be quite accurate. Agreement between total cross sections calculated exactly by QED Feyman graphs and by EPA has been found at the level of $\simeq 5\%$ [15]. There is general agreement in the literature on the expression (7) for the total equivalent photon spectrum in leading log approximation. Problems, however, arise if the factorization approach is used when tagging is done at angles $m_e/E \ll \theta \ll 1$. This has recently been pointed out by Carimolo et al., in a study where direct comparisons were made between cross sections calculated in EPA and by QED for

μ-pair production. Writing the condition (12), that the factorizable equations (13b) and (13c) follow from eq. (11), in terms of angles and scaled electron energies

$$z^2 \gg (1-x_i)\sin^2\tfrac{1}{2}\theta_i\,, \qquad i=1,2\,,$$

it is clear that either $1-x_i \simeq 0$ or if x_i is small, $z \gg \frac{1}{2}\theta_i$. The first case, though presumably mathematically possible, is of little physical interest due to the sharp fall off of the luminosity function with increasing z (see fig. 2). It is still of interest to note, however, that a factorizable region with very loose angular restrictions should exist near $z=1$. This region of factorizability is completely outside the classical Weizsäcker–Williams [7–9] kinematical region where it is required that the virtual photon energy is $\ll$beam energy. Of more physical interest is the case $z \gg \frac{1}{2}\theta_i$, x_i small. However, practical limitations require that typically $\theta > 10$ mrad, so to be confident of neglecting the Q^2 terms, say $z \geq 0.05$ is needed and for $\theta >$ 200 mrad no region of validity for deriving the factorizable formulae remains. In the study of ref. [16] it was found that in order to keep deviations from the QED result less than a factor 2 for particular kinematical configurations when using a Weizsäcker–Williams luminosity function corresponding to eqs. (13c) and (15), it was required that (in the notation of this paper)

$$Q/z \leqslant \tfrac{1}{6}.$$

Unlike in the case of the total equivalent photon spectrum a number of significantly different expressions have appeared in the literature for the photon flux in a limited angular region: $\mathrm{d}N_\gamma/\mathrm{d}x(x, \theta_{\min}, \theta_{\max})$. Arteaga-Romero et al. [1] found an expression identical to eq. (15). Brodsky et al. [2], gave the spectrum

$$\frac{\mathrm{d}N_\gamma^{\mathrm{BKT}}}{\mathrm{d}x}(x, \theta_{\min}, \theta_{\max}) = \left(\frac{\alpha}{\pi}\right)\frac{1}{x}\left\{[1+(1-x)^2]\ln\frac{\theta_{\max}}{\theta_{\min}} - \frac{(2-x)^2}{4}\ln\frac{[x^2+(1-x)\theta_{\max}^2]}{[x^2+(1-x)\theta_{\min}^2]}\right\}, \tag{16}$$

while more recently Carimalo et al. [17], have derived the spectrum, appropriate only to the case of single tagging:

$$\frac{\mathrm{d}N_\gamma^{\mathrm{CKP}}}{\mathrm{d}x}(x, \theta_{\min}, \theta_{\max}) = \left(\frac{\alpha}{\pi}\right)\frac{1}{x}\left\{[1+(1-x)^2]\ln\frac{\theta_{\max}}{\theta_{\min}} - (1-x)\ln\frac{D(x,\theta_{\max})}{D(x,\theta_{\min})} - 4\frac{x(1-x)(\theta_{\max}^2-\theta_{\min}^2)}{D(x,\theta_{\min})D(x,\theta_{\max})}\right\}, \tag{17}$$

where

$$D(x,\theta) \equiv 4x + (1-x)\theta^2\,.$$

As pointed out earlier [5] and recently reiterated in ref. [17], the spectrum (16), derived correctly for the case of electroproduction on nucleons, is not appropriate to

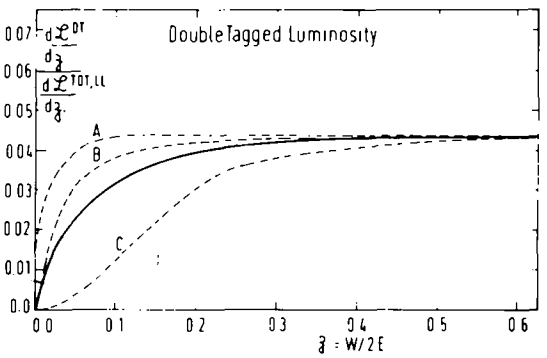

Fig. 7. Double tagging efficiency curves. $E = 15$ GeV, $20 < \theta_1, \theta_2 < 200$ mrad. Solid line: from eq. (9). Dashed line: EPA calculations. A: eqs. (13c), (15); B: eqs. (13c), (17); C: eqs. (13c), (16).

the two-photon collision process because of different kinematical conditions. Use of formula (16) has led to a number of erroneous calculations of tagging efficiency for two-photon processes in the last year or so*.

Comparison of the luminosity functions calculated via eqs. (13b) and (13c) using eq. (7) for dN_γ^{TOT}/dx and eqs. (15), (16) or (17) for $dN_\gamma(x_1\ \theta_{min}, \theta_{max})/dx$ are shown in figs. 7 and 8 for double and single tagging respectively. Also shown are the functions calculated from eqs. (9) and (11). The angular range taken is 20–200 mrad and $E = 15$ GeV. $d\mathcal{L}/dz$ is found from eqs. (13b), (13c) by substituting $x_2 = z^2/x_1$ from eq. (8) and numerically integrating over x_1 between the limits z^2 and 1. Strictly speaking, eq. (17) should not be used to give the equivalent photon spectrum for double tagging. However, it is interesting to note that it agrees much more closely

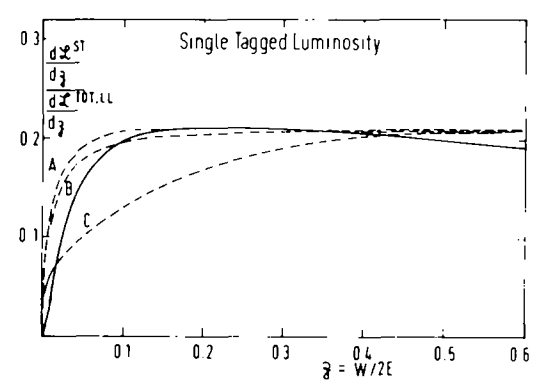

Fig. 8. Single tagging efficiency curve. $E = 15$ GeV, $20 < \theta_2 < 200$ mrad. Solid line: from eq. (11). Dashed line: EPA calculation. A: eqs. (13b), (15); B: eqs. (13b), (17); C: eqs. (13b), (16).

* Eq. (16) was quoted by the author in ref. [21] and has been used in several ECFA/LEP reports for tagging efficiency calculations. It has also been widely used in calculations made in support of experimental proposals.

with the curve calculated from eq. (9) than eqs. (15) or (16). The maximum discrepancy is ≈20% near $z = 0.1$. Eq. (15) shows a discrepancy larger by a factor of ≈2. Eq. (17) is then useful even for double tagging calculations if only a rough estimate of the tagging efficiency is required as it is much easier to carry out the single integration over x_1 than the 4-dimensional integration needed if the exact expression, eq. (9), is used. For single tagging the agreement between eqs. (11), (15), (17) is good, better than 10% for $z > 0.05$. At smaller values of z, (15) and (17) overestimate the luminosity quite seriously, but, as discussed above, one should not expect factorizable formulae to be valid in this region. As can be seen in both figs. 7 and 8, the incorrect formula (16) rather grossly underestimates the luminosity for $z \leqslant 0.3$.

7. Rapidity distributions of differential luminosity

If the leading log approximation, eq. (7), is made to the total virtual photon flux, and eq. (15) is taken for the photon flux in the angular range $\theta_{\min} < \theta < \theta_{\max}$, all luminosity functions, untagged, single tagged and double tagged, have a simple functional form in terms of scaled effective mass of the two photon system and its rapidity in the lab system y:

$$\frac{\mathrm{d}^2\mathscr{L}}{\mathrm{d}y\,\mathrm{d}z} = \frac{\mathrm{d}^2\mathscr{L}}{\mathrm{d}y\,\mathrm{d}z}\bigg|_{z=1} \frac{[1+(1-z\,\mathrm{e}^{y})^2][1+(1-z\,\mathrm{e}^{-y})^2]}{z}. \tag{8}$$

Eq. (18) follows from eqs. (13) and the definition of rapidity

$$y \equiv \frac{1}{2}\ln\frac{E+p_z}{E-p_z} \tag{19}$$

on neglecting the angles of the virtual photons relative to the beams and using the simplified relation, eq. (8), for z. The ratio

$$\frac{\mathrm{d}^2\mathscr{L}}{\mathrm{d}y\,\mathrm{d}z} \Big/ \frac{\mathrm{d}^2\mathscr{L}}{\mathrm{d}y\,\mathrm{d}z}\bigg|_{z=1}$$

is plotted as a function of y for various values of z in fig. 9. A plateau develops in the differential luminosity as z is decreased from 1. The length of the plateau is $y_{\max} = \ln(1/z)$ and the height becomes $\propto 1/z$ as $z \to 0$. For small values of z there is an almost uniform distribution in rapidity from 0 to $y_{\max}$.

8. Effects of experimental acceptance on the luminosity functions

In order to reduce backgrounds to tolerable levels when studying 2γ processes in e^+e^- storage rings it is normal to require the detection of at least one particle, from the system X produced in the two-photon annhilation, in the experimental detector. With a few simplifying assumptions it is fairly straightforward to make a rough

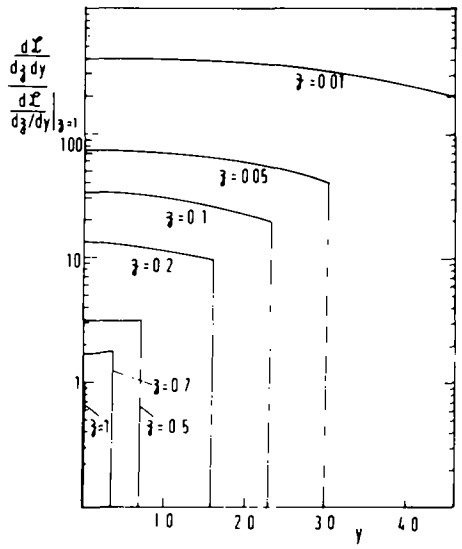

Fig. 9. Differential luminosity distributions as a function of rapidity in the lab of the two-photon system, y, for various fixed values of z.

estimate of the reduction in effective luminosity resulting from such cuts. If the produced system consists of relativistic particles in its barycentric frame then a particle emitted at 90° to the direction of motion of X in this frame will appear in the lab at an angle $1/\beta\gamma$, independent of the particle momentum, where β and γ are the relativistic velocity and energy of the system X in the lab. Furthermore, in the approximation $\beta \simeq 1$, a given range of c.m. angles, say

$$\tfrac{1}{4}\pi < \theta^* < \tfrac{3}{4}\pi \tag{20}$$

will appear in the lab above a certain minimum angle $\theta^{\mathrm{L}}_{\min}$, where for the angular range (20) corresponding to $\simeq 70\%$ of the c.m. solid angle $\theta^{\mathrm{L}}_{\min} \simeq 0.41/\gamma$. Relaxing the restriction $\beta \simeq 1$ will increase $\theta^{\mathrm{L}}_{\min}$ from this value. Requiring that one particle is seen in the lab at an angle $> \theta^{\mathrm{L}}_{\min}$ is then equivalent to one particle appearing in the range (20) of c.m. angle. If the probability of the latter is near 100%, which would be the case, if for example, the system X was massive $J^{PC} \equiv 0^{+}$ state decaying into many pions, then the relation between $\theta^{\mathrm{L}}_{\min}$ and γ can be inverted to give an estimate of the accepted luminosity. So for a fixed angular cut in the lab, $\theta > \theta_c$ it follows from the above argument that there is a maximum value of γ, $\gamma_{\max} = 0.41/\theta_c$, such that all particles omitted in at least the c.m. angular range (20) are detected in the lab. For larger values of γ, a smaller range of c.m. angles is accepted and the acceptance correspondingly falls. 70% of the c.m. solid angle is taken as a reasonable definition of the "shoulder" of the acceptance function. Neglecting the angles of the virtual

photons relative to the beam, the relativistic velocity of the system X is given by

$$\beta = \frac{p}{E} = \frac{x_1 - x_2}{x_1 + x_2}. \tag{21}$$

The restriction $\beta < \beta_{\max}$ where $\beta_{\max} = \sqrt{\gamma_{\max}^2 - 1}/\gamma_{\max}$ is then translated directly into a restriction on the range of integration of the variable x_1 (it is assumed here that z is fixed and $x_2 = z^2/x_1$) and so the change in the luminosity function is directly calculable. This is shown in fig. 4. The allowed region of x_1 lies between A and B along the curve $z^2 = x_1 x_2$, where A and B are the intersections with this curve of lines

$$x_2 = \frac{(1-\beta_{\max})}{(1+\beta_{\max})} x_1 \ (\mathrm{OL}), \qquad \text{and} \qquad x_2 = \frac{(1+\beta_{\max})}{(1-\beta_{\max})} x_1 \ (\mathrm{OL}').$$

The limits of the x_1 integration are changed from

$$z^2 \to 1$$

to

$$z\sqrt{\frac{1-\beta_{\max}}{1+\beta_{\max}}} \to z\sqrt{\frac{1+\beta_{\max}}{1-\beta_{\max}}}$$

by the restriction $\beta < \beta_{\max}$. Evidently, if $z > \sqrt{(1-\beta_{\max})/(1+\beta_{\max})}$, kinematics requires that $\beta < \beta_{\max}$ anyway, the x_1 integration is from $z^2 \to 1$ and the luminosity function is unmodified. This can be seen in fig. 4 since in this case there are no intersections A, B of the lines OL, OL' with $z^2 = x_1 x_2$ in the allowed regions $0 \leq x_{1,2} \leq 1$.

The luminosity restriction given by the condition $\beta < \beta_{\max}$ changes dramatically with the angular cut θ_c. Taking $\theta_c = 20$ mrad (technically feasible for a forward detector) gives $(1-\beta_{\max})/(1+\beta_{\max}) = 6 \times 10^{-4}$, and so no luminosity restriction for $z > 0.024$. $\theta_c = 300$ mrad, a typical minimum angle for a central (solenoidal) detector, gives $(1-\beta_{\max})/(1+\beta_{\max}) = 0.19$ and so loss of luminosity occurs for $z < 0.44$. This value is taken for the lines OL, OL' shown in fig. 4. The corresponding modification of the luminosity function is shown in fig. 10. Here eqs. (13c) and (17) (factorizable formulae) were used. The angular range taken for the scattered electrons is $20 < \theta < 200$ mrad but the fractional reduction in luminosity, ε_β, given by the β cut is almost independent of this, and using the simpler form eq. (15) for $(\mathrm{d}N_\gamma/\mathrm{d}x)(x, \theta_{\min}, \theta_{\max})$ would be strictly independent of $\theta_{\min}$ and $\theta_{\max}$. In this case it is, in fact, given by the analytical expression:

$$\varepsilon_\beta = \frac{(2+z^2)^2 \ln(1/\alpha^2) - 2z(1/\alpha - \alpha)[2z^2 - z(1/\alpha + \alpha) + 4]}{(2+z^2)^2 \ln(1/z^2) - 2(1-z^2)(3+z^2)}, \tag{22}$$

where

$$\alpha = \sqrt{\frac{1-\beta_{\max}}{1+\beta_{\max}}}.$$

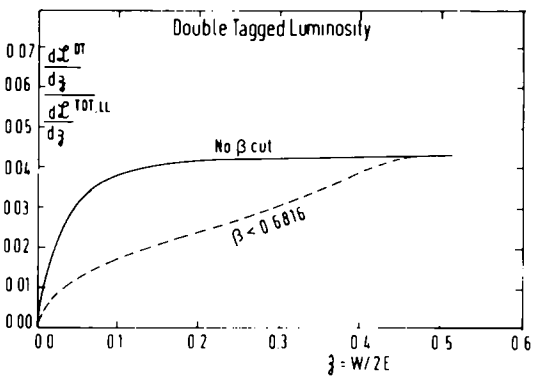

Fig. 10. Double tagging efficiency curves. $E = 15$ GeV, $20 < \theta_1, \theta_2 < 300$ mrad. Solid line: from eqs. (13c), (17); no restriction on β. Dashed line: $\beta < 0.682$ or $\theta_c = 300$ mrad.

It is evident that even in the case considered here of an almost isotropic distribution of final-state particles in the barycentric frame of X, there is a large loss of effective luminosity in changing the minimum accepted angle of the detector from 20 to 300 mrad. Further loss of acceptance will occur if the produced particles are forward and backward peaked in the centre of mass system for dynamical seasons as will be the case for many final states of interest. This clearly indicates the importance of good experimental acceptance in the forward direction. Such forward acceptance is particularly important to observe low mass final states with good efficiency.

9. Conclusions and closing remarks

(a) Total luminosity. The agreement between the simple leading log expressions and the full luminosity function is quite good, except near $z = 1$ (fig. 3), the leading log approximation typically overestimates the luminosity by 10–15%.

(b) Tagged luminosity. There are significant differences between the double and single tagged luminosity functions given by eqs. (9) and (11), respectively, and those previously appearing in the literature, derived using the factorizable EPA approach. In particular, the formula given in ref. [2], whose validity has previously been questioned [5, 17] strongly underestimates the luminosity at small values of z. The equivalent photon spectrum recently calculated by Carimalo et al. [17], gives the best agreement with the present calculations in both the singly and doubly tagged case.

(c) Acceptance effects. In the case where detection of at least one produced particle is required, it is important to have acceptance in the angular range below 300 mrad, to study two-photon processes with good efficiency, particularly for small values of the effective mass of the produced system.

The terms of reference of this study have been somewhat limited, but it is hoped at least to have quantified the differences between what may be called unpolarized transverse photon approximation, i.e., the assumptions (i) to (iii) of sect. 1 plus the exact helicity formula, and the factorizable EPA type of calculation. The validity of

the latter type of approximation has been tested by comparison with exact QED calculations for various kinematical regions in a series of recent papers [16, 18]. The same authors have also given an analysis of single tagged processes where the restriction to transverse photons is dropped [19]. To perform more precise calculations, short of making a full Feyman diagram computation, requires relaxing assumptions (i) and/or (ii) of sect. 1, i.e., making some physics assumptions about the virtual $\gamma\gamma$ process. Such an approach within the EPA philosophy has recently been taken by Olsen [20]. For the case of the total hardonic cross section where at low Q^2 the photon-hadron coupling is expected to be via a vector meson propagator, it is straightforward to modify eq. (9) by a simple multiplicative factor in Q^2 to account for this [21]. For processes where the photon coupling is pointlike*, a strong dependence on Q^2 of the photon-photon cross section is not expected and more significant errors might be expected to come from the restriction to transverse photons.

The work described here as benefited largely from discussions with and communications from A. Courau, M. Defrise, F. Gutbrod, J. Reignier and P. Kessler.

Appendix

The functions $F^{(1)}(E/m_e, \sigma)$, $F^{(2)}(\sigma)$ are given in appendix 2 of ref. [4] as

$$F^{(1)} = 4(1+\tfrac{1}{2}\sigma)^2 \ln\frac{1}{\sigma}\left(\ln\frac{W}{m_e}\right)^2 - 2(1-\sigma)(3+\sigma)\left[\ln\frac{W}{m_e}(1-\sigma)\right]^2$$

$$+2\ln\frac{W}{m_e}\left(\ln\frac{1}{\sigma}\right)^2(2+\sigma+\sigma^2)$$

$$+\{\tfrac{1}{2}(1-\sigma)(39+3\sigma)-8(1+\tfrac{1}{2}\sigma)^2[L_2(1)-L_2(\sigma)]\}\ln\frac{W}{m_e}(1-\sigma)$$

$$-\ln\frac{W}{m_e}\ln\frac{1}{\sigma}(14-4\sigma-5\sigma^2),$$

$$F^{(2)} = [\tfrac{2}{3}(1+\tfrac{1}{2}\sigma)^2+\tfrac{1}{4}\sigma^2]\left(\ln\frac{1}{\sigma}\right)^3 - 4(1+\tfrac{1}{2}\sigma)\ln\frac{1}{\sigma}[\ln(1-\sigma)]^2$$

$$-(4-\tfrac{5}{4}\sigma^2)\left(\ln\frac{1}{\sigma}\right)^2 - 2(1-\sigma)(3+\sigma)\ln\frac{1}{\sigma}\ln(1-\sigma)$$

$$+\{\tfrac{17}{2}-31\sigma-\tfrac{19}{2}\sigma^2+6(1+\sigma+\tfrac{5}{12}\sigma^2)L_2(1)+6(1+\tfrac{1}{2}\sigma)^2L_2(\sigma)$$

$$+12(1+\sigma)[a(\sigma)]^2\}\ln\frac{1}{\sigma},$$

* The pointlike coupling may arise either because lepton pairs are produced in the final state or, in hadronic processes, where an internal quark line is far from mass-shell. See ref. [22].

where

$$L_2(\sigma) = \sum_{n=1}^{\infty} \frac{\sigma^n}{n^2}, \qquad L_2(1) = \tfrac{1}{6}\pi^2,$$

$$a(\sigma) = \tfrac{1}{6}\pi - \arctan\sqrt{\frac{\sigma}{4-\sigma}}.$$

Note that although $F^{(1)}$ is written above in terms of W/m_e and σ, this equivalent to E/m_e and σ since

$$\ln\frac{W}{m_e} = \ln\frac{2E}{m_e}\frac{W}{2E} = \ln\frac{E}{m_e} - \tfrac{1}{2}\ln\sigma + \ln 2.$$

References

[1] N. Arteaga-Romero, A. Jaccarini, P. Kessler and J. Parisi, Phys. Rev. D3 (1971) 1569.
[2] S.J. Brodsky, T. Kinoshita and H. Terazawa, Phys. Rev. D4 (1971) 1532.
[3] V.M. Budnev, V.L. Chernyak and I.F. Ginzberg, Nucl. Phys. B34 (1971) 470.
[4] G. Bonneau, M. Gourdin and F. Martin, Nucl. Phys. B54 (1973) 573.
[5] V.M. Budnev et al., Phys. Reports 15 (1974) 182.
[6] A. Courau, 1975 PEP Summer Study Report SLAC-190, LBL-4800, p. 159.
[7] E. Fermi, Z. Phys. 29 (1924) 315.
[8] C.F. v. Weizsäcker, Z. Phys. 88 (1934) 612.
[9] E.J. Williams, Proc. Roy. Soc. A139 (1933) 163; Phys. Rev. 45 (1934) 729.
[10] L.D. Landau and E.M. Lifshitz, Phys. Z. Sov. 6 (1934) 244.
[11] D. Kessler and P. Kessler, Nuovo Cim. 4 (1956) 601.
[12] R.B. Curtis, Phys. Rev. 104 (1956) 211.
[13] R.H. Dalitz and D.R. Yennie, Phys. Rev. 105 (1957) 1598.
[14] F.E. Low, Phys. Rev. 120 (1960) 582.
[15] R. Bhattacharya, J. Smith and G. Grammer, Phys. Rev. D15 (1977) 3267;
F. Gutbrod and Z.J. Rek, Z. Phys. C1 (1979) 171.
[16] C. Carimalo, P. Kessler and J. Parisi, Collège de France preprint L.P.C. 79-06, Phys. Rev., to be published.
[17] C. Carimalo, P. Kessler and J. Parisi, Collège de France preprint, A Dalitz-Yennie type equivalent photon spectrum for $\gamma\gamma$ collisions in electron storage rings (August, 1979) Phys. Rev. Lett., submitted.
[18] C. Carimalo, P. Kessler and J. Parisi, Collège de France preprint, L.P.C. 79-09, On the analysis of virtual $\gamma\gamma$ collision processes in the deep inelastic configuration (June, 1979) Phys. Rev., submitted.
[19] C. Carimalo, P. Kessler and J. Parisi, On the interpretation of singly tagged events in $\gamma\gamma$ experiments, Collège de France preprint (August, 1979) Phys. Rev., submitted.
[20] H. A. Olsen, Phys. Rev. D19 (1979) 100.
[21] J.H. Field, Proc. LEP Summer Study CERN 79-01, p. 580.
[22] S.J. Brodsky, T.A. de Grand, J.F. Gunion and J.H. Weis, Phys. Rev. Lett. 41 (1978) 672;
C.H. Llewellyn-Smith, Phys. Lett. 79B (1978) 83;
K. Kajantie, Physica Scripta 19 (1979) 230.